Homodimetallic iron(II) hydrazones: syntheses, spectroscopic, electrochemical, and theoretical investigations. X-Ray crystal structure of both *syn*- and *anti*- rotamers of $[(\eta^5\text{-Cp})Fe(\eta^6\text{-}C_6H_5)\text{–}NHN{=}C(Me)\text{–}(\eta^5\text{-}C_5H_4)\ Fe(\eta^5\text{-Cp})]^+PF_6^-$

Carolina Manzur,*[a] Mauricio Fuentealba,[a] Lorena Millán,[a] Francisco Gajardo,[a] David Carrillo,*[a] Jose A. Mata,[b] Sourisak Sinbandhit,[c] Paul Hamon,[d] Jean-René Hamon,*[d] Samia Kahlal[e] and Jean-Yves Saillard*[e]

[a] *Laboratorio de Química Inorgánica, Universidad Católica de Valparaíso, Avenida Brasil 2950, Valparaíso, Chile*
[b] *Departamento de Química Inorgánica y Orgánica, Universitat Jaume I, E-12080, Castellón, Spain*
[c] *Centre Régional de Mesures Physiques de l'Ouest, Université de Rennes 1, Campus de Beaulieu, F-35042, Rennes cedex, France*
[d] *Laboratoire Organométalliques et Catalyse: Chimie et Electrochimie Moléculaires, (CNRS UMR 6509), Institut de Chimie de Rennes, Université de Rennes 1, Campus de Beaulieu, F-35042 Rennes cedex, France*
[e] *Laboratoire de Chimie du Solide et Inorganique Moléculaire (CNRS UMR 6511), Institut de Chimie de Rennes, Université de Rennes 1, Campus de Beaulieu, 35042 Rennes cedex, France*

Received (in Strasbourg, France) 7th August 2001, Accepted 17th October 2001
First published as an Advance Article on the web

Two homogeneous series of homodimetallic iron(II) hydrazone complexes of general formula $[CpFe(\eta^6\text{-p-}RC_6H_4)\text{–}NHN{=}CH\text{–}(\eta^5\text{-}C_5H_4)FeCp]^+PF_6^-$ ($Cp = \eta^5\text{-}C_5H_5$): R = H, [**5**]$^+PF_6^-$; Me, [**6**]$^+PF_6^-$; MeO, [**7**]$^+PF_6^-$; Cl, [**8**]$^+PF_6^-$; and $[CpFe(\eta^6\text{-p-}RC_6H_4)\text{–}NHN{=}CMe\text{–}(\eta^5\text{-}C_5H_4)FeCp]^+PF_6^-$: R = H, [**9**]$^+PF_6^-$; Me, [**10**]$^+PF_6^-$; MeO, [**11**]$^+PF_6^-$, have been prepared. These hydrazones were stereoselectively obtained as their *trans* isomers about the N=C double bond, by reaction of the corresponding organometallic hydrazines $[CpFe(\eta^6\text{-}p\text{-}RC_6H_4NHNH_2)]^+PF_6^-$, R = H, [**1**]$^+PF_6^-$; Me, [**2**]$^+PF_6^-$; MeO, [**3**]$^+PF_6^-$; and Cl, [**4**]$^+PF_6^-$, with formylferrocene, $CpFe(\eta^5\text{-}C_5H_4\text{–}CHO)$, and acetylferrocene, $CpFe(\eta^5\text{-}C_5H_4\text{–}CO\text{-}Me)$, respectively. All the new compounds were characterized by elemental analysis and IR, UV-Vis and ^{1}H NMR spectroscopies. For compound [**9**]$^+PF_6^-$, the activation energy $\Delta G^{\#}$ for the hindered rotations of the mixed sandwich $[CpFe(\eta^6\text{-}C_6H_5\text{–})]^+$ (41.8 ± 0.9 and 41.2 ± 3.7 kJ mol^{-1}) and the ferrocenyl unit (40.0 ± 3.2 kJ mol^{-1}) about the –NH–N=CMe– hydrazone backbone have been determined by variable temperature ^{1}H NMR spectroscopic studies. The electrochemical behavior of the dinuclear hydrazones was explored by cyclic voltammetry, and features the role of the cationic $[CpFe(\eta^6\text{-arene})]^+$ moiety as an electron acceptor. The crystalline and molecular structure of [**9**]$^+PF_6^-$ was determined by single crystal X-ray crystallographic analysis. The structure shows the presence of both *syn* and *anti* rotamers in the asymmetric unit. The analysis of the electronic structure of [**9**]$^+$ through DFT calculations indicate a strong perturbation of the metal centers by the hydrazone bridge as well as some metal-metal interaction through the bridge.

During the last decade, metal-containing π-conjugated systems have emerged as a important category of materials because these kinds of complexes are expected to possess physical properties significantly different from their organic conjugated counterparts.[1] This has led to a growing development of organometallic push-pull rod-shapped oligomers, which are mainly metallocene-based donor-acceptor materials, and the topic has been the subject of recent reviews.[2] Along this line, dinuclear M-Fe complexes, M = Cr, Mo, W,[1q,3] and Ru,[4] where the electron-accepting (η^6-arene)metal moieties are linked to the ferrocenyl unit by conjugated spacers, have recently been described, and some of them exhibit interesting NLO properties.[1q,3a,4] Likewise, mixed sandwich compounds such as the cationic derivatives $[CpFe(\eta^6\text{-arene})]^+$ ($Cp = \eta^5\text{-}C_5H_5$) have proven to be robust electron acceptors,[5] and also to have very useful redox properties that allow electronic interaction between ligand-bridged metals.[6]

Hydrazones possess a zigzag π-conjugated core that can be capped with an organometallic donor-acceptor pair. In a previous paper,[7] we have performed the complexation of one aromatic ring of a free organic hydrazone with the 12-electron organometallic moiety $FeCp^+$, a cationic fragment that is as electron withdrawing as two nitro groups on an arene ring,[8] to obtain the first π-coordinated organometallic hydrazone derivatives of the type $[CpFe(\eta^6\text{-}C_6H_4R\text{–}NHN{=}CMe_2)]^+$ (R = H, Me, MeO, Cl). In this contribution we describe an extension of this work with (*i*) the synthesis and characterization of two homogeneous series of new homodimetallic hydrazone

DOI: 10.1039/b107631k

This journal is © The Royal Society of Chemistry and the Centre National de la Recherche Scientifique 2002

complexes of the general formulae [CpFe(η^6-*p*-RC_6H_4)–NHN=CH–(η^5-C_5H_4)FeCp]$^+PF_6^-$ (R = H, [**5**]$^+PF_6^-$; Me, [**6**]$^+PF_6^-$; MeO, [**7**]$^+PF_6^-$; Cl, [**8**]$^+PF_6^-$) and [CpFe(η^6-*p*-RC_6H_4)–NHN=CMe–(η^5-C_5H_4)FeCp]$^+PF_6^-$ (R = H, [**9**]$^+PF_6^-$; Me, [**10**]$^+PF_6^-$; MeO, [**11**]$^+PF_6^-$); (*ii*) the electrochemical and solvatochromic behavior of these seven new dinuclear hydrazone compounds; (*iii*) the crystal structure of both *syn*- and *anti*-rotamers of compound [**9**]$^+PF_6^-$ that are present in the same asymmetric unit, and its solution dynamics that reveal the two rotational barriers of the sandwich moieties about the –N(H)–N=C(Me)– spacer; and (*iv*) finally, DFT calculations on the [**9**]$^{2+/+/0}$ series as well as on related mononuclear models, which provide a theoretical rationalization of the electronic interaction between the metal centers. Some of the experimental results have been previously communicated.[9]

Results and discussion

Synthesis and characterization of homodimetallic hydrazone complexes

The synthesis of two new series of bis-iron(II) hydrazone complexes, as their PF_6^- salts, [CpFe(η^6-*p*-RC_6H_4)–NHN=CR′–(η^5-C_5H_4)FeCp]$^+$ (R, R′ = H, H [**5**]$^+$; Me, H [**6**]$^+$; MeO, H [**7**]$^+$; Cl, H [**8**]$^+$; H, Me [**9**]$^+$; Me, Me [**10**]$^+$; MeO, Me [**11**]$^+$), was accomplished by the reaction between their respective organometallic hydrazine precursors [CpFe(η^6-*p*-RC_6H_4–$NHNH_2$)]$^+PF_6^-$ [**1**–**4**]$^+PF_6^-$ and formyl- or acetylferrocene, respectively, in the presence of glacial acetic acid in ethanol (Scheme 1). It is interesting to note that this synthetic methodology that we have successfully applied for the preparation of mononuclear organometallic hydrazones,[7] also appears to conveniently give access to homodimetallic hydrazone counterparts. However, all attempts to react the *p*-chlorophenylhydrazine precursor, [**4**]$^+PF_6^-$, with acetylferrocene were unsuccessful. An untractable oily residue was always obtained whatever the experimental conditions used.

All the organometallic hydrazones [**5**–**11**]$^+PF_6^-$ were obtained as air stable yellow-orange microcrystalline solids in yields ranging from 57 to 79%. They exhibit high solubility in CH_2Cl_2, MeCN, Me_2CO, DMSO, and are fairly light-sensitive in solution. The identities of these seven new homodimetallic hydrazones were inferred from satisfactory elemental analyses, ^{1}H NMR, IR and UV-Vis spectroscopies (see Experimental), and a crystalline and molecular structure determination of [**9**]$^+PF_6^-$ (*vide infra*).

The IR spectra of these seven powdered compounds invariably exhibit (*i*) a sharp, weak to medium absorption band in the 3320 to 3360 cm^{-1} region, which has been attributed to the stretching mode of the N–H bond;[10] (*ii*) a sharp intense band in the region from 1560 to 1580 cm^{-1}, corresponding to the stretching mode of the C=N group; and (*iii*) a very strong $\nu(PF_6)$ band between 830 and 860 cm^{-1}, which in some cases is observed as two, well-resolved absorption bands, as well as a sharp, strong ν(P–F) band at 550–560 cm^{-1}. Interestingly, the spectrum of a crystalline sample of [**9**]$^+PF_6^-$ shows *two* N–H stretching frequencies at 3368 and 3322 cm^{-1}, compatible with the presence of the *syn* and *anti* rotamers revealed by the X-ray crystal structure (*vide infra*). In contrast, only one N–H absorption at 3344 cm^{-1} is observed in CH_2Cl_2 at room temperature. This is consistent with the most stable isomer, presumably *anti*, being the predominant species present in solution (see Theoretical investigations below).

The dinuclear organometallic hydrazone species are indeed stereoselectively formed as their *trans* isomer as demonstrated by the unique pattern of their ^{1}H NMR spectra (acetone-d_6, 297 K), and on the basis of NOE experiments on [**9**]$^+PF_6^-$ (see Experimental). Typically, the ^{1}H NMR spectra feature (*i*) two different singlets for the C_5H_5 ring protons, in the 4.15–4.45 ppm region for CpFe and 4.80–5.25 ppm region for $CpFe^+$; (*ii*) two unresolved pseudo-triplets for the Hα and Hβ proton resonances of the –C_5H_4 group; the downfield-shifted signal (δ 4.66–4.99) being assigned to the Hα proton from NOE experiments; (*iii*) a broad signal in the 8.40–9.70 ppm range attributed to the –NH– proton resonance, which is observed at low field due to the electron-withdrawing properties of the [FeCp]$^+$ cationic moiety linked to the phenyl ring; (*iv*) a proton resonance in the 7.90–8.10 ppm region, assigned to the azomethine fragment, –N=CH–, in the case of hydrazones [**5**–**8**]$^+PF_6^-$ derived from formylferrocene, and a resonance in the 2.17–2.33 ppm range attributed to the methyl group of the –N=CMe– fragment in the case of hydrazones [**9**–**11**]$^+PF_6^-$ derived from acetylferrocene.

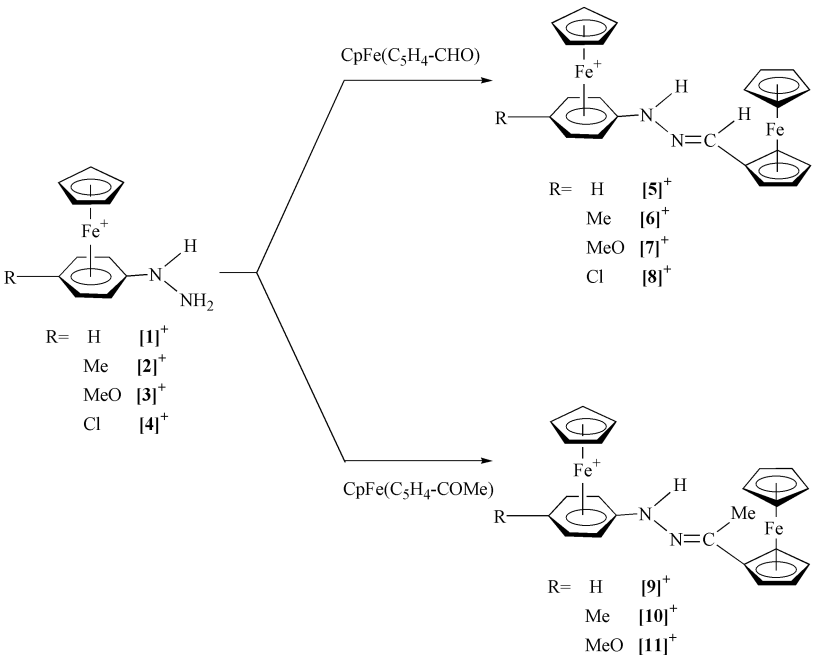

Scheme 1

Solution dynamics

The peculiar solid-state behavior of complex $[\mathbf{9}]^+PF_6^-$, illustrated by its infrared spectrum and its crystal structure (*vide infra*), prompted us to investigate its solution behavior. Variable-temperature ^1H NMR spectroscopic studies were conducted in the temperature range 173–296 K. Dynamic processes involving the $[CpFe(\eta^6\text{-}C_6H_5)]^+$ phenyl group [Fig. 1(a)] as well as the C_5H_4 group of the ferrocenyl moiety [Fig. 1(b)] were readily seen, whereas all other parts of the NMR spectrum were temperature invariant. In the low-temperature (173 K) limiting spectrum of the phenyl region, the two doublets at δ 6.36 and 5.97 are attributable to the diastereotopically related H_o and $H_{o'}$ protons, whereas the two overlapping triplets at δ 5.94 and 5.90 are assigned to the diastereotopic H_m and H_m'. When the temperature is raised, the overlapping triplets first broaden at *ca.* 189 K and then transform into a single triplet at δ 5.97. Next, the $H_o$and $H_{o'}$ doublets broaden, coalesce at 214 K, and finally give a single doublet at δ 6.28 at 296 K. The free energies of activation for these two exchange processes were calculated at their coalescence temperatures from eqn. (1)[11] and found to be 41.8 ± 0.9 and 40.2 ± 3.7 kJ mol^{-1} for the H_o/H_o' and H_m/H_m' systems, respectively:

$$\Delta G^{\#} = RT_c(22.96 + \log_N T_c/\Delta\nu)$$
$$(\text{in J mol}^{-1},\ R = 8.31\ \text{J K}^{-1},\ T_c \text{ in K},\ \nu \text{ in Hz}) \quad (1)$$

Similar observations are found for the diastereotopic H_α and $H_{\alpha'}$ protons of the C_5H_4 ring (H_β and $H_{\beta'}$ were not resolved). The two broad signals attributed to H_α and $H_{\alpha'}$ at δ 4.62 and 4.57 in the low-temperature limiting spectrum undergo coalescence at 189 K and then transform into a sharp triplet at δ 4.69 at 296 K. The activation free energy for this process was calculated as 40.0 ± 3.2 kJ mol^{-1}.

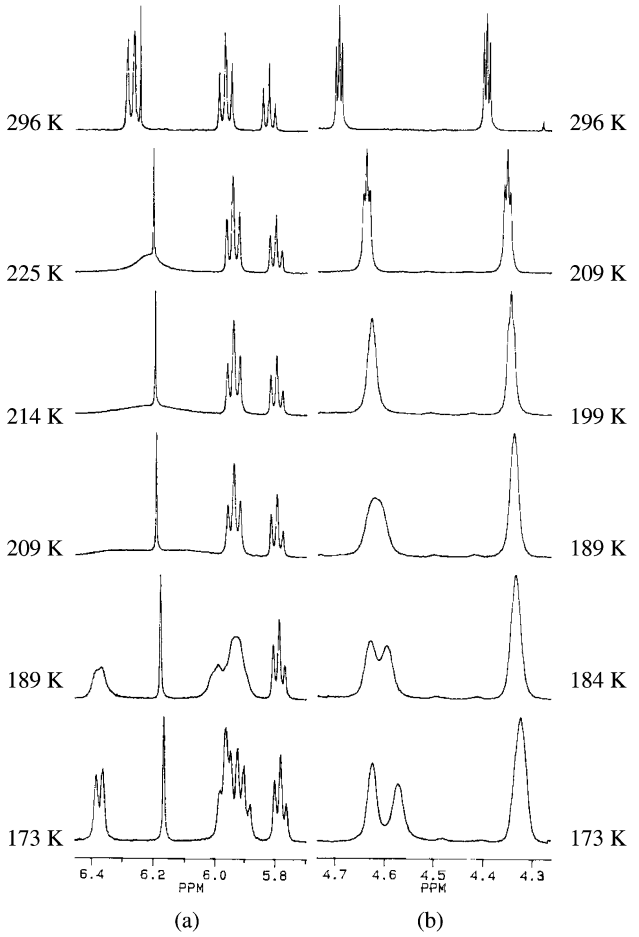

Fig. 1 High-field ^1H NMR spectra (300 MHz) of $[CpFe(\eta^6\text{-}C_6H_5)\text{–}NHN{=}C(Me)\text{–}(\eta^5\text{-}C_5H_4)FeCp)]^+PF_6^-$ ($[\mathbf{9}]^+PF_6^-$) at various temperatures in CD_2Cl_2: (a) H_{ortho} and H_{meta} (C_6H_5), (b) H_α (C_5H_4).

The variable-temperature NMR observations are readily explained in terms of rotation of the cationic mixed sandwich $[CpFe(\eta^6\text{-}C_6H_5\text{–})]^+$ unit around the C_{Phenyl}–N bond and of the ferrocenyl fragment around its C_5H_4–C linkage to the hydrazone core. We will assume in the following that only one of the rotamers of $[\mathbf{9}]^+$ (presumably the *anti*, see Theoretical investigations for a discussion) is present in solution. This is supported by the facts that (*i*) only one IR ν(N–H) band was seen in solution, and (*ii*) ^1H NMR signals due to only one species were detected over the temperature range 173–296 K. It is important to note that because H_o and H_o' are diastereotopic, a rotation around the C_{Phenyl}–N bond alone will never cause the coalescence of the H_o and $H_{o'}$ signals, irregardless of the rate of this rotation. The same applies to the coalescence of the H_m and $H_{m'}$ signals. Similarly, a fast rotation around the C_5H_4–C bond alone will not cause the interconversion of the diastereotopic H_α and $H_{\alpha'}$ protons. However, if the dynamic behavior involves rotation around the C_{Phenyl}–N and the C_5H_4–C bonds, then coalescence may result: the combined rotation around the two bonds will cause the interconversion of one enantiomer of $[\mathbf{9}]^+$, which has a plane of chirality at each of the metal moieties, into the other enantiomer with consequential exchange of the local environments of H_o and H_o', H_m and H_m', and H_α and $H_{\alpha'}$. It is sufficient for rationalizing the observed behavior that one of the rotational processes has a high barrier. In the absence of obvious severe steric interactions, this is most likely to be the rotation around the C_{Phenyl}–N bond, which has significant double-bond character, as inferred from the X-ray structure and the theoretical calculations (*vide infra*). In this way, the dynamic process starting from one *anti* enantiomer of $[\mathbf{9}]^+$ involves (*i*) slow rotation around the C_{Phenyl}–N bond by 180 degrees to give the unobserved, less stable *syn* rotamer or isomer, followed by (*ii*) rapid rotation around the C_5H_4–C bond by 180 degrees to give the *anti* rotamer as the opposite enantiomer of that initially present (the opposite order of events will of course have the same effect).

X-Ray crystallographic study of $[\mathbf{9}]^+PF_6^-$

The single crystal X-ray diffraction study of the bimetallic hydrazone complex $[CpFe(\eta^6\text{-}C_6H_5)\text{–}NHN{=}C(Me)\text{–}(\eta^5\text{-}C_5H_4)FeCp]^+PF_6^-$, $[\mathbf{9}]^+PF_6^-$, was undertaken and the crystal structure was determined as outlined in the Experimental. The ORTEP plots of the cationic organometallic *syn*- and *anti*-rotamers, *syn*-$[\mathbf{9}]^+$ and *anti*-$[\mathbf{9}]^+$, with the atom labelling scheme, are given in Fig. 2, and selected intramolecular distances and angles are presented in Table 1.

The coordination geometry at the iron atoms and the bond distances and angles are essentially similar in the two rotamers (Table 1). In each case, the metrical parameters are typical of η^5-Fe-η^6 and η^5-Fe-η^5 metallocene-type coordination.[12–14] The carbocyclic rings coordinated to the same iron center are essentially parallel with one another, and the ring centroid–iron–ring centroid vectors are almost collinear in both the $[Cp\text{–}Fe\text{–}arene]^+$ and ferrocenic fragments (Table 1). Similarly to previous observations,[4,7,15,16] high anisotropic thermal motion and/or disorder was noted not only in the carbon atoms of the Cp ligand of the mixed sandwiches but also in the Cp ligands of the ferrocenyl moieties. The observed orientations are presumably due to partial rotation of the C_5 rings about the Fe–Cp (centroid) axes.

The most noticeable feature of this crystalline structure is the presence of both *syn*- and *anti*-rotamers in the same asymmetric unit. The *syn*-$[\mathbf{9}]^+$/*anti*-$[\mathbf{9}]^+$ interconversion occurs by rotation of either the $[CpFe(\eta^6\text{-}C_6H_5)\text{–}]^+$ fragment around the C_{phenyl}–N bond, that is C(6)–N(6) and C(56)–N(56), or of

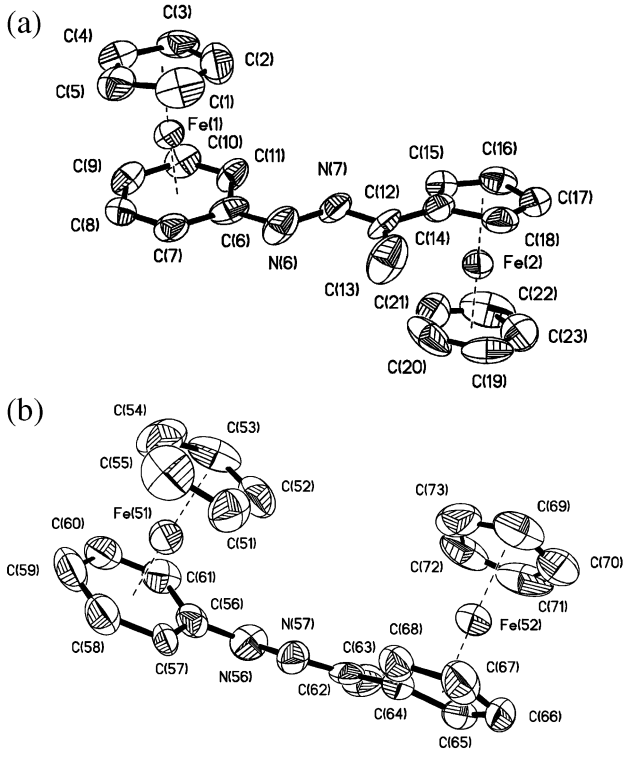

Fig. 2 Molecular structure of *anti*-[**9**]$^+$ (a) and *syn*-[**9**]$^+$ (b), showing the atom numbering scheme. Hydrogen atoms and counter anion PF_6^- have been omitted for clarity. Thermal ellipsoids are drawn at 50% probability. This figure shows the two different rotamers found for compound [**9**]$^+PF_6^-$ in the same asymmetric unit.

the ferrocenyl unit around C(12)–C(14) or C(62)–C(64), in agreement with the two rotational barriers observed in the variable temperature NMR studies (see above). To the best of our knowledge, [**9**]$^+PF_6^-$ is the first bis-sandwich complex showing this peculiar arrangement in the solid state. *Syn*- and *anti*-rotamers are indeed known for complexes of fulvalene[17] and polyarene[18] coordinating two $Cp'Fe^+$ ($Cp' = C_5H_5$ or C_5Me_5) moieties but in all cases reported, the sterically less encumbered *anti* isomer is the unique one found in the solid state.

On the other hand, structural data indicate π-electron delocalization along the bent hydrazone skeleton backbone, through (*i*) the slight cyclohexadienyl-like character at the coordinated C_6 phenyl rings[19,20] with folding angles of 3.6(1)° and 3.1(1)° for the *syn*-[**9**]$^+$ and *anti*-[**9**]$^+$, respectively; (*ii*) some C_{phenyl}–N multiple bond character as in C(6)–N(6) = 1.377(10) and C(56)–N(56) = 1.376(11) Å;[21] (*iii*) the depyramidalization of the N(6) and N(56) benzylic-type nitrogen atom, which is reflected by typical bond angles at the sp^2-hybridized nitrogen atom: C(6)–N(6)–N(7) = 119.6(8)° and C(56)–N(56)–N(57) = 115.2(8)° for *anti*-[**9**]$^+$ and *syn*-[**9**]$^+$, respectively; and (*iv*) a short carbon-carbon single bond linking the ferrocenyl unit to the hydrazone core: C(12)–C(14) = 1.452(12) and C(62)–C(64) = 1.476(12) Å.

Finally, considering that the lack of planarity of the conjugated spacer decreases the electronic interaction between the donor and acceptor metal centers, we have calculated the deviation from planarity, defined as the dihedral angle between the two C_6 and C_5 rings, of the anionic binucleating ligand $[(C_6H_5)–NH–N=CMe–(C_5H_4)]^-$, in both *syn*-[**9**]$^+$ and *anti*-[**9**]$^+$ rotamers. These values are 41.98(36)° and 10.85(51)°, respectively. Surprisingly, this dihedral angle observed in *anti*-[**9**]$^+$ is one-third of that measured for $[CpFe(\eta^6\text{-}p\text{-}MeO–C_6H_4–NH–N=CH–(\eta^5\text{-}C_5H_4)FeCp]^+PF_6^-$, [**7**]$^+PF_6^-$, of similar structure,[22] indicating that in the present case not steric strains between the methyl group and the α-hydrogen atoms of the C_5H_4 group but rather crystal packing forces might be substantially more important in controlling the solid state structures or conformations of both rotamers (Fig. 2).

Electrochemical studies

In order to get a deeper insight into the mutual donor-acceptor electronic influence, we studied the electrochemical behavior of the homodimetallic hydrazones derived from formylferrocene, [**5**–**8**]$^+PF_6^-$, and acetylferrocene, [**9**–**11**]$^+PF_6^-$, by cyclic voltammetry (CV). The voltammograms of the seven compounds under investigation exhibit similar patterns, and the electrochemical data, including those of ferrocene measured under the same conditions, are listed in Table 2.

Table 1 Selected bond distances (Å) and angles (°) of *anti*- and *syn*-rotamers of complex [**9**]$^+$ [a]

anti-[**9**]$^+$		*syn*-[**9**]$^+$	
Fe(1)–C(6)	2.159(9)	Fe(51)–C(56)	2.138(10)
Fe(1)–C(7–11)[b]	2.074	Fe(51)–C(57–61)[b]	2.076
C(6)–N(6)	1.377(10)	C(56)–N(56)	1.376(11)
N(6)–N(7)	1.382(9)	N(56)–N(57)	1.390(9)
N(7)–C(12)	1.300(10)	N(57)–C(62)	1.270(10)
C(12)–C(13)	1.500(11)	C(62)–C(63)	1.500(11)
C(12)–C(14)	1.452(12)	C(62)–C(64)	1.476(12)
C–C(Cp′)[b]	1.409	C–C(Cp′)[b]	1.418
Fe(1)–Fe(2)	9.72(10)[c]	Fe(51)–Fe(52)	9.71(2)[c]
	7.75(6)[d]		6.48(4)[d]
Fe(1)–Cp_{CNT}	1.65(4)	Fe(51)–Cp_{CNT}	1.66(3)
Fe(2)–Cp_{CNT}	1.65(5)	Fe(52)–Cp_{CNT}	1.66(5)
Fe(1)–Ph_{CNT}	1.54(3)	Fe(51)–Ph_{CNT}	1.55(3)
Fe(2)–Cp'_{CNT}	1.65(4)	Fe(52)–Cp'_{CNT}	1.65(3)
C(6)–N(6)–N(7)	119.6(8)	C(56)–N(56)–N(57)	115.2(8)
N(6)–N(7)–C(12)	117.1(8)	N(56)–N(57)–C(62)	117.5(8)
N(7)–C(12)–C(14)	115.2(9)	N(57)–C(62)–C(64)	114.5(8)
N(7)–C(12)–C(13)	124.2(9)	N(57)–C(62)–C(63)	126.9(9)
C(14)–C(12)–C(13)	120.7(9)	C(64)–C(62)–C(63)	118.6(9)
Cp_{CNT}–Fe(1)–Ph_{CNT}	176.90(9)	Cp_{CNT}–Fe(51)–Ph_{CNT}	178.5(3)
Cp_{CNT}–Fe(2)–Cp'_{CNT}	177.35(10)	Cp_{CNT}–Fe(52)–Cp'_{CNT}	178.0(5)

[a] Abbreviations: $Cp = C_5H_5$, $Cp' = C_5H_4$, $Ph = C_6H_5$, CNT = centroid. [b] Average bond distance. [c] Sum of the bond distances. [d] Measured through-space distances.

Table 2 Electrochemical data[a]

Compound	E_{pc}[b]/V	E^0[c]/V	ΔE_p[d]/mV
[**5**]$^+PF_6^-$	−1.43	0.60	87
[**6**]$^+PF_6^-$	−1.46	0.57	89
[**7**]$^+PF_6^-$	−1.38	0.56	68
[**8**]$^+PF_6^-$	−1.50	0.57	88
[**9**]$^+PF_6^-$	−1.41	0.53	64
[**10**]$^+PF_6^-$	−1.59	0.53	76
[**11**]$^+PF_6^-$	−1.54	0.55	78
$(C_5H_5)_2Fe$	—	0.44	68

[a] In dry MeCN at 298 K with 0.1 M *n*-$Bu_4N^+PF_6^-$ as supporting electrolyte; all potentials are *vs.* Ag/AgCl; scan rate = 0.1 V s^{-1}. [b] Peak potential of the irreversible wave corresponding to the reduction of the $[CpFe(arene)]^+$ fragment. [c] Potentials are taken as the midpoints between anodic and cathodic peaks. [d] Peak-to-peak separation between the resolved reduction and oxidation wave maxima.

All the complexes [**5**–**11**]$^+PF_6^-$ undergo a reversible one-electron oxidation in the range 0.53 to 0.60 V *vs.* Ag/AgCl. This anodic process is centered at the ferrocenyl group, (η^5-C_5H_4)FeCp, of the homodimetallic hydrazones, and corresponds to the generation of the dicationic Fe(II)/Fe(III) mixed-valence species. All mono-/dication redox processes in Table 2 were chemically reversible, near-Nernstian processes (ΔE_p = 64–89 mV). The E^0 values of the reversible one-electron oxidations are positively shifted by 0.09–0.16 V with respect to that of ferrocene, thus illustrating the electron-withdrawing properties of the cationic [CpFe(η^6-*p*-RC_6H_4–NHN=C(R′)–)]$^+$ entity. A more positive oxidation potential indicates that the ferrocenyl unit is more difficult to oxidise, that is less electron rich. In contrast, an irreversible reduction process, in the range −1.38 to −1.59 V *vs.* Ag/AgCl, is observed for the seven compounds examined. This cathodic process is centered at the $[CpFe(\eta^6\text{-arene})]^+$ moiety and corresponds to the generation of the unstable 19-electron Fe(I)Fe(II) species.[23] This electrochemical behavior is in agreement with the HOMO being essentially ferrocene based while the character of the LUMO is dominated by the cationic sandwich $[CpFe(\eta^6\text{-arene})]^+$, and is fully consistent with the theoretical results (see below). Participation of the hydrazone core –N(H)–N=C(R′)– (R′ = H, Me) to the electron delocalization that will perturb the redox potential shifts must also be envisioned.[24] One effect is illustrated by the substitution of a methyl group for a hydrogen one (Table 2). Complexes [**9**–**11**]$^+PF_6^-$ are indeed easier to oxidise (mean value 0.54 V) than [**5**–**8**]$^+PF_6^-$ (mean value 0.57 V), and conversely, are more difficult to reduce. However, in the specific case of [**9**]$^+PF_6^-$ the role of the electron-accepting moiety $[CpFe]^+$ is clearly evidenced when comparing the oxidation potentials of the mono- and dinuclear species.[24] Compound [**9**]$^+PF_6^-$ is more difficult to oxidize by 60 mV than its corresponding mononuclear derivative.

On the other hand, the influence of the substituent groups on the phenyl rings seems to be weak by comparison with the electron delocalization from the (η^5-C_5H_4)FeCp group toward the $[CpFe(\eta^6\text{-arene})]^+$ fragment, so that a meaningful correlation between E^0 or E_{pc} and the Hammett substituent constants, σ_p-X, could not be obtained.

All these electrochemical data taken together support electronic interaction to some extent between the electron-donating and -accepting termini for the homodimetallic hydrazones [**5**–**11**]$^+PF_6^-$.[25]

Electronic absorption spectra

The UV-vis spectra of complexes [**5**–**11**]$^+PF_6^-$ have been recorded in CH_2Cl_2 (μ = 8.90) and DMSO (μ = 47.6) (see Experimental). The data are consistent with the behavior of most ferrocenyl monosubstituted compounds reported in the literature in that they show two charge-transfer bands in the visible region.[1*h*,*n*,*o*,2,3*a*,4,26] The complexes exhibit, in CH_2Cl_2, a prominent absorption band in the range 300–320 nm assigned to π-π* transitions (ILCT). This band is blue-shifted in complexes [**5**–**8**]$^+PF_6^-$ in DMSO by 3–6 nm, while in complexes [**9**–**11**]$^+PF_6^-$, this band is red-shifted 4–6 nm in the same solvent. On the other hand, the broad lower energy band, observed in the range 400–525 nm, is attributed to a donor-acceptor charge-transfer transition. This is in agreement with theoretical results[27] and with the previously cited experimental work, although the assignment may be controversial.[28] The broadening of this low-energy band is probably the result of the overlap of broad d-d visible bands corresponding to both the $[CpFe(\eta^6\text{-arene})]^+$[29] and ($\eta^5$-$C_5H_4$)$FeCp$[30] fragments. This band is blue-shifted in all complexes in DMSO. However, the magnitude of this hypsochromic effect in these complexes could not be accurately determined due to the difficulty of assigning with sufficient accuracy their λ_{max} values.

Theoretical investigations

In order to provide a rationalization of the structure and properties of the title compounds, we have carried out DFT calculations on the real compound [**9**]$^+$, as well as on its reduced and oxidized forms, [**9**] and [**9**]$^{2+}$, respectively. An analysis of the interaction between the metal centers has been performed by comparing the DFT results of the [**9**]$^{0/+/2+}$ series with those obtained on the mononuclear hydrazone complexes $[CpFe(\eta^5\text{-}C_5H_4)\text{–}CMeNNH_2]^{0/+}$ and $[CpFe(\eta^6\text{-}C_6H_5)\text{–}NHNCHMe]^{+/0}$. Calculations were carried out both in the local density approximation (LDA) and with the Becke and Perdew (BP) non-local corrections applied (see Experimental). The LDA and BP calculations lead to very similar results, except that the BP optimized Fe–C distances were found to be ≈3% longer than the LDA ones, which are closer to the experimental values. For these reasons, we show only the LDA optimized metrical data in Table 3.

Two stable conformations were found for [**9**]$^+$, corresponding to the *anti* and *syn* conformations. These optimized geometries are very similar to the experimentally determined X-ray structures (see Table 3). The *anti* conformation is found to be more stable than its *syn* rotamer by 0.08 eV and 0.15 eV at the LDA and BP levels, respectively. This small energy difference is in agreement with the two isomers being in equilibrium at room temperature and fully consistent with the NMR data. The *anti* and *syn* conformations were also found to be isomers for the reduced [**9**] and oxidized [**9**]$^{2+}$ forms. In the case of [**9**], the *anti* conformation is found to be the most stable by 0.07 eV and 0.12 eV at the LDA and BP levels, respectively, as is also the case for [**9**]$^{2+}$ (by 0.12 eV at the LDA level).

The 3 highest occupied MO's of both rotamers of [**9**]$^+$ can be identified as being the 3d-type weakly bonding or antibonding "t_{2g}" orbitals of the ferrocenyl metal center [83–97% Fe(2/52)], while the "t_{2g}" orbitals of the second metal center lie at lower energy. On the other hand, the 2 lowest unoccupied MO of [**9**]$^+$ are the 3d-type metal-ligand antibonding "e_g*" orbitals of the η^5-Fe-η^6 unit [57% Fe(1/51)]. These results are consistent with the fact that oxidation and reduction of [**9**]$^+$ are expected to occur at the η^5-Fe-η^5 and η^5-Fe-η^6 centers, respectively (see above). More surprisingly, the antibonding "e_g*" MO of the η^5-Fe-η^6 unit were found to have a significantly larger localization on the Cp ligand than on the C_6 ring (28% *vs.* 15%). This polarization on the C_5 ring is at variance with what is generally found for $[(\eta^5\text{-}C_5R_5)Fe(\eta^6\text{-}C_6R'_6)]^+$ complexes.[20,31] It is attributable to the strong donor ability of the hydrazone ligand, which strongly destabilizes the π manifold of the phenyl ring. It follows that, when [**9**]$^+$ is reduced to [**9**], the Fe–C(Cp) distances of the η^5-Fe-η^6 unit undergo a larger increase than the Fe–C(C_6 ring) distances (see

Table 3 Major optimized structural data (distances in Å, angles in °) computed at the LDA level for $[\mathbf{9}]^{0/+/2+}$, $[CpFe(\eta^5\text{-}C_5H_4)\text{–}CMeNNH_2]^{0/+}$ and $[CpFe(\eta^6\text{-}C_6H_5)\text{–}NHNCHMe]^{0/+}$. The corresponding X-ray data found for $[\mathbf{9}]^+$ are given in brackets

	anti-$[\mathbf{9}]^q$			*syn*-$[\mathbf{9}]^q$			$[CpFe\text{-}(\eta^5\text{-}C_5H_4)\text{–}CMeNNH_2]^q$		$[CpFe(\eta^6\text{-}C_6H_5)\text{–}NHNCHMe]^q$	
	$q=2+$	$q=1+$	$q=0$	$q=2+$	$q=1+$	$q=0$	$q=1+$	$q=0$	$q=1+$	$q=0$
Fe(2/52)–C(Cp)	2.064	2.041 [2.020]	2.041	2.071	2.041 [2.035]	2.046	2.065	2.035		
Fe(2/52)–C(C_5H_4R)	2.070	2.031 [2.036]	2.034	2.066	2.034 [2.045]	2.042	2.065	2.032		
C–C(Cp) av. [Fe(2/52) unit]	1.424	1.424 [1.369]	1.425	1.421	1.427 [1.387]	1.424	1.421	1.424		
C–C(C_5H_4R) av. [Fe(2/52) unit]	1.422	1.426 [1.408]	1.428	1.420	1.426 [1.418]	1.426	1.424	1.426		
Fe(1/51) –C(Cp)	2.056	2.047 [2.033]	2.100	2.058	2.053 [2.033]	2.155			2.057	2.122
Fe(1/51)–C(C_6 ring)	2.087	2.088 [2.088]	2.107	2.089	2.084 [2.086]	2.106			2.097	2.109
Fe(1/51)–C(6/56)	2.126	2.197 [2.159]	2.289	2.141	2.146 [2.137]	2.201			2.203	2.216
C–C(Cp) av. [Fe(1/51) unit]	1.421	1.422 [1.398]	1.421	1.420	1.421 [1.387]	1.426			1.420	1.420
C–C(C_6 ring) av. [Fe(1/51) unit]	1.410	1.412 [1.406]	1.412	1.410	1.411 [1.402]	1.424			1.409	1.411
C(14/64)–C(12/62)	1.440	1.438 [1.453]	1.436	1.442	1.440 [1.475]	1.437	1.434	1.449		
C(12/62)–N(7/57)	1.304	1.300 [1.300]	1.305	1.303	1.293 [1.270]	1.300	1.308	1.288	1.280	1.288
N(7/57)–N(6/56)	1.323	1.344 [1.382]	1.331	1.324	1.348 [1.389]	1.341	1.299	1.349	1.342	1.328
N(6/56)–C(6/56)	1.369	1.346 [1.377]	1.359	1.366	1.356 [1.376]	1.372			1.352	1.374
N(6/56)–N(7/57)–C(12/62)	119	118 [117]	119	119	120 [118]	120	120	120	119	120
$\Sigma\alpha_{N(6/56)}$	360	360 [360]	359	360	357 [360]	353	360	341	360	359
$\Sigma\alpha_{C(12/62)}$	360	360 [360]	360	360	360 [360]	360	360	360	360	360
C(6/56)–N(6/56)–N(7/57)–C(12/62)	180	178 [179]	173	179	176 [175]	175			175	173
N(6/56)–N(7/57)–C(12/62)–C(13/63)	1	−5 [−3]	−3	0	−6 [−4]	−4	0	1	−2	−1

Table 3). The reduction is also accompanied by an increase of the cyclohexadienyl-like character of the coordinated C_6 ring. On the other side, the η^5-Fe-η^5 unit is barely changed upon reduction. In comparison, when $[\mathbf{9}]^+$ is oxidized to $[\mathbf{9}]^{2+}$, it is the η^5-Fe-η^5 unit that is mainly concerned. An elongation of the Fe–C distances by $\approx$ 1–2% is found, in agreement with the weak bonding character of the $[\mathbf{9}]^+$ HOMO.

An evaluation of the interaction that occurs between the metal centers through the hydrazone bridge can be provided by a comparison of the DFT results of $[\mathbf{9}]^+$ with those obtained for the mononuclear species generated by the replacement of one of the sandwich units of $[\mathbf{9}]^+$ by a hydrogen atom, namely $[CpFe(\eta^5\text{-}C_5H_4)\text{–}CMeNNH_2]$ and $[CpFe(\eta^6\text{-}C_6H_5)\text{–}NHNCHMe]^+$. On average, the Fe–C distances involving the η^5-Fe-η^5 metal are slightly longer in $[\mathbf{9}]^+$ than in its mononuclear parent. The opposite effect is found for the Fe–C distances involving the η^5-Fe-η^6 moiety. This can be tentatively interpreted as the result of some electron donation from weakly bonding "t_{2g}" occupied orbitals of the η^5-Fe-η^5 fragment of $[\mathbf{9}]^+$ into unoccupied antibonding orbitals of the η^5-Fe-η^6 fragment. However, a comparison of the Mulliken charges of $[\mathbf{9}]^+$ with those of its mononuclear parents do not indicate any significant charge transfer. Moreover, the ionization potentials of [**9**] and $[CpFe(\eta^6\text{-}C_6H_5)\text{–}NHNCHMe]$, calculated as the energy differences of the optimized structures of the cationic and neutral species, indicate that $[\mathbf{9}]^+$ is slightly less difficult to reduce than its mononuclear parent (by $\approx$ 0.04 eV, at both LDA and BP levels). The ionization potentials of both the *anti* and *syn* conformations of [**9**] are nearly the same ($\approx$ 4.1 eV at both LDA and BP levels). This value is close to that calculated by the same method for $(\eta^5\text{-}C_5Me_5)Fe(\eta^6\text{-}C_6Me_6)$.[31b] Unfortunately, it is not possible to rationalize the difference between the calculated ionization potentials of $[\mathbf{9}]^+$ and $[CpFe(\eta^5\text{-}C_5H_4)\text{–}CMeNNH_2]$ in terms of electronic effects because these compounds bear different charges. The value computed for the mononuclear species are 6.92 and 6.59 eV at the LDA and BP levels, respectively. They compare well with that computed for ferrocene (7.11 eV).[20] The geometry of the hydrazone unit in the mononuclear species is quite similar to the one found for $[\mathbf{9}]^+$, except that in $[CpFe(\eta^5\text{-}C_5H_4)\text{–}CMeNNH_2]$, the N(6/56) atom, no longer conjugated with a phenyl ring, is significantly pyramidalized. A comparison of $[CpFe(\eta^5\text{-}C_5H_4)\text{–}CMeNNH_2]$ and $[CpFe(\eta^6\text{-}C_6H_5)\text{–}NHNCHMe]^+$ with their respective one-electron oxidized and reduced forms shows similar structural trends as when comparing $[\mathbf{9}]^+$ with $[\mathbf{9}]^{2+}$ and [**9**].

Taken as a whole, these results are indicative of a weak but significant interaction between the iron centers.

Concluding remarks

We have presented a facile synthetic methodology leading to two new homogeneous series of homodimetallic hydrazones that can be viewed as non-rod-shaped dipolar chromophores. To the best of our knowledge, complex $[\mathbf{9}]^+PF_6^-$ represents the first crystallographically characterized example of a homodimetallic hydrazone. Its X-ray structure shows a very peculiar arrangement, with both *anti* and *syn* rotamers in the asymmetric unit. It is noteworthy that in these complexes the neutral moiety CpFe and its oxidized form $CpFe^+$ act as donor and acceptor groups, respectively, while the binucleating anionic hydrazone skeleton spacer $[(\eta^6\text{-}p\text{-}RC_6H_4)\text{–}NHN{=}CR'\text{–}(\eta^5\text{-}C_5H_4)]^-$ (R′ = H, Me) acts as a bridging ligand, allowing the electronic interaction between both iron centers through the delocalized π system. Structural, electrochemical and computational (DFT) data confirm the ground state electronic interaction between the mixed sandwich [CpFe(arene)]$^+$ and ferrocene-based termini. Further work will be directed to an inprovement of the electron delocalization by linkage of electron-withdrawing groups to the arene ring and electron-releasing substituents at the ferrocene, and in the determination of the potential NLO properties of these new bimetallic complexes.

Experimental

General

All operations were performed under an inert atmosphere using standard vacuum/nitrogen line (Schlenk) techniques. Solvents were dried and distilled under nitrogen by standard methods prior to use. Reagents were obtained as follows: ferrocene, formylferrocene, acetylferrocene were purchased

from commercial sources and used as received. The hydrazine complexes $[CpFe(\eta^6\text{-}C_6H_5NHNH_2)]^+PF_6^-$, $[\mathbf{1}]^+PF_6^-$, $[CpFe(\eta^6\text{-}p\text{-}MeC_6H_4NHNH_2)]^+PF_6^-$, $[\mathbf{2}]^+PF_6^-$ and $[CpFe(\eta^6\text{-}p\text{-}MeOC_6H_4NHNH_2)]^+PF_6^-$, $[\mathbf{3}]^+PF_6^-$, were prepared according to our previously published procedure.[7] Melting points were determined in evacuated capillaries and were not corrected. Microanalytical data were obtained on a Perkin–Elmer Model 2400 elemental analyzer. IR spectra were obtained as KBr disks on a Perkin–Elmer Model 1600 FT-IR spectrophotometer. Electronic spectra were recorded in CH_2Cl_2 and DMSO solutions with a Spectronic Genesys 2 spectrophotometer.

^{1}H NMR spectra were recorded on a multinuclear Bruker DPX 200 spectrometer (200 MHz) at 297 K and all chemical shifts are reported in ppm relative to internal tetramethylsilane or the proton resonance resulting from incomplete deuteration of the NMR solvent. Variable-temperature ^{1}H NMR spectra were recorded on a Bruker AM300WB spectrometer at 300 MHz. Temperatures within the NMR probe were controlled by a Bruker VT unit; temperature calibration was accomplished by following the Van Geet methanol calibration method[32] and found to be accurate to within 1 °C. NOE experiments were carried out in acetone-d_6 on a Bruker AM300WB spectrometer (300 MHz) at 297 K. Samples for NOE experiments are prepared as follows: 10 mg of the compound was dissolved in 1 ml of CD_3COCD_3 in a finger-type Schlenk tube and degassed by a very slow bubbling of argon under ultrasonic irradiation for 20 min. The orange-yellow solution was then filtered into a degassed NMR tube and the spectra were immediately run.

Cyclic voltammetry studies were carried out with a home-made potentiostat of conventional design, using a standard three-electrode setup with platinum working and auxiliary electrodes and a Ag/AgCl reference electrode. Acetonitrile solutions were 1.0 mM for the compound under study and 0.1 M for the supporting electrolyte n-$Bu_4N^+PF_6^-$. Under these experimental conditions the Cp_2Fe/Cp_2Fe^+ couple was located at 0.44 V.

Syntheses

$[CpFe(\eta^6\text{-}p\text{-}ClC_6H_4NHNH_2)]^+PF_6^-$, $[\mathbf{4}]^+PF_6^-$. The synthesis of this complex was carried out using a procedure similar to that we have described elsewhere,[7] using in this case a mixture of 416 mg (1.00 mmol) of $[CpFe(\eta^6\text{-}p\text{-}ClC_6H_4Cl)]^+PF_6^-$,[33] and 0.3 ml (6.0 mmol) of $NH_2NH_2{\cdot}H_2O$ in 5.0 ml of CH_2Cl_2. Recrystallization of the crude product from CH_2Cl_2–Et_2O (1 : 1) provided a yellow-orange crystalline solid. Yield 108 mg (26%), m.p. 135 °C. $C_{11}H_{12}ClF_6FeN_2P$ (408.49): calcd. C, 32.34; H, 2.96; found C, 32.60; H, 3.19. UV/Vis (CH_2Cl_2): λ_{max} (log ε) 250 nm (4.26), 326 (3.26), 408 (2.67). IR (KBr): ν 3416 cm^{-1} (m) ν(NH); 3374 (m) ν(NH); 3115, 3088 (w) ν(CH); 2928, 2862 (vw) ν(CH); 1556 (s) δ(NH); 834 (br, vs) $\nu(PF_6)$ and 558 (s) δ(P–F). ^{1}H NMR (CD_3COCD_3): $\delta = 2.96$ (br s, 2H, NH_2), 5.18 (s, 5H, C_5H_5), 6.47 (d, 2H, C_6H_4, $J_{H\text{-}H} = 6.9$ Hz), 6.70 (d, 2H, C_6H_4, $J_{H\text{-}H} = 6.9$ Hz), 8.89 (br s, 1H, NH).

$[CpFe(\eta^6\text{-}C_6H_5)\text{–}NHN{=}CH\text{–}(\eta^5\text{-}C_5H_4)FeCp]^+PF_6^-$, $[\mathbf{5}]^+PF_6^-$. To 32.1 mg (0.150 mmol) of formylferrocene, $CpFe(\eta^5\text{-}C_5H_4\text{–}CHO)$, dissolved in 3.0 ml of EtOH, 56.2 mg (0.150 mmol) of $[\mathbf{1}]^+PF_6^-$ and one drop of glacial acetic acid were added. The solution was refluxed for 4.5 h. The clean reaction mixture was allowed first to stand at room temperature and then at −30 °C overnight. The orange crystalline solid formed was filtered off and washed with cold EtOH. Finally, the complex was recrystallized from CH_2Cl_2–Et_2O (1 : 1). Yield 51 mg (59%), m.p. 165 °C (dec). $C_{22}H_{21}F_6Fe_2N_2P$ (414.12): calcd. C, 46.35; H, 3.71; found C, 45.96; H, 3.64. UV/Vis (CH_2Cl_2): λ_{max} (log ε) 242 nm (4.39), 247 (413, sh), 317 (4.23), 454 (3.41); (DMSO): λ_{max} (log ε) 320 nm (4.15), 340 (4.11, sh), 430 (3.35). IR (KBr): ν 3324 cm^{-1} (m) ν(NH); 3005 (w) ν(CH); 2955 (vw) and 2919 (w) ν(CH); 1572 (s) ν(C=N); 848 (br, vs) $\nu(PF_6)$ and 559 (s) δ(P–F). ^{1}H NMR (CD_3COCD_3): $\delta = 4.36$ (s, 5H, CpFe), 4.57 (br t, 2H, H_β–C_5H_4), 4.88 (br t, 2H, H_α–C_5H_4), 5.14 (s, 5H, $CpFe^+$), 6.21–6.37 (m, 5H, Ph), 8.08 (s, 1H, CH), 9.50 (br s, 1H, NH).

$[CpFe(\eta^6\text{-}p\text{-}MeC_6H_4)\text{–}NHN{=}CH\text{–}(\eta^5\text{-}C_5H_4)FeCp]^+PF_6^-$, $[\mathbf{6}]^+PF_6^-$. The synthesis of this orange complex was carried out using a procedure similar to that described for complex $[\mathbf{5}]^+PF_6^-$, using in this case 32.6 mg of formylferrocene (0.15 mmol) and 58.4 mg (0.150 mmol) of $[\mathbf{2}]^+PF_6^-$. Yield 50 mg (57%), m.p. 154 °C (dec). $C_{23}H_{23}F_6Fe_2N_2P$ (584.10): calcd. C, 47.29; H, 3.97; found C, 46.92; H, 3.85. UV/Vis (CH_2Cl_2): λ_{max} (log ε) 242 nm (4.31), 314 (4.19), 340 (4.03, sh), 451 (3.38); (DMSO): λ_{max} (log ε) 318 nm (4.18), 340 (4.10, sh), 426 (3.38). IR (KBr): ν 3326 cm^{-1} (m) ν(NH); 3092 (w) ν(CH); 2975, 2924 (vw) ν(CH); 1570 (s) ν(C=N); 850, 830 (vs) $\nu(PF_6)$ and 556 (m) δ(P–F). ^{1}H NMR (CD_3COCD_3): $\delta = 2.54$ (s, 3H, CH_3), 4.34 (s, 5H, CpFe), 4.54 (br t, 2H, H_β–C_5H_4), 4.86 (br t, 2H, H_α–C_5H_4), 5.10 (s, 5H, $CpFe^+$), 6.33 (d, 2H, C_6H_4, $J_{H\text{-}H} = 6.9$ Hz), 6.28 (d, 2H, CH_4, $J_{H\text{-}H} = 6.9$ Hz), 8.07 (s, 1H, CH), 9.49 (br s, 1H, NH).

$[CpFe(\eta^6\text{-}p\text{-}MeOC_6H_4)\text{–}NHN{=}CH\text{–}(\eta^5\text{-}C_5H_4)FeCp]^+PF_6^-$, $[\mathbf{7}]^+PF_6^-$. The synthesis of this yellow-orange complex was carried out using a procedure similar to that described for complex $[\mathbf{5}]^+PF_6^-$, using in this case 61.3 mg (0.29 mmol) of formylferrocene and 99.9 mg (0.25 mmol) of $[\mathbf{3}]^+PF_6^-$. Yield 117.9 mg (79%), m.p. 162 °C (dec). $C_{23}H_{23}F_6Fe_2N_2OP$ (600.10): calcd. C, 46.03; H, 3.86; found C, 45.82; H, 3.78. UV/Vis (CH_2Cl_2): λ_{max} (log ε) 240 nm (4.38), 309 (4.24), 344 (3.96, sh), 425 (3.46); (DMSO): λ_{max} (log ε) 313 nm (4.18), 345 (3.98, sh), 405 (br). IR (KBr): ν 3337 cm^{-1} (m) ν(NH); 3100 (w) ν(CH); 2926, 2840 (w) ν(CH); 1579 (s) ν(C=N); 1254 (m) ν(C–O); 852, 844 (br, vs) $\nu(PF_6)$, 558 (m) δ(P–F). ^{1}H NMR (CD_3COCD_3): $\delta = 4.08$ (s, 3H, OCH_3), 4.43 (s, 5H, CpFe), 4.64 (br t, 2H, H_β–C_5H_4), 4.94 (br t, 2H, H_α–C_5H_4), 5.13 (s, 5H, $CpFe^+$), 6.30 (d, 2H, C_6H_4, $J_{H\text{-}H} = 7.3$ Hz), 6.25 (d, 2H, C_6H_4, $J_{H\text{-}H} = 7.3$ Hz), 8.01 (s, 1H, CH), 9.30 (br s, 1H, NH).

$[CpFe(\eta^6\text{-}p\text{-}ClC_6H_4)\text{–}NHN{=}CH\text{–}(\eta^5\text{-}C_5H_4)FeCp]^+PF_6^-$, $[\mathbf{8}]^+PF_6^-$. This red-orange complex was synthesized according to the procedure described above for $[\mathbf{5}]^+PF_6^-$, using in this case 52 mg (0.25 mmol) of formylferrocene and 100 mg (0.25 mmol) of $[\mathbf{4}]^+PF_6^-$. Yield 113 mg (76%), m.p. 165 °C (dec). $C_{22}H_{20}ClF_6\ Fe_2N_2P$ (604.51): calcd. C, 43.71; H, 3.33; found C, 43.81; H, 3.48. UV/Vis (CH_2Cl_2): λ_{max} (log ε) 245 nm (4.44), 268 (4.20, sh), 315 (4.28), 475 (3.50); (DMSO): λ_{max} (log ε) 321 nm (4.17), 342 (4.12, sh), 449 (3.40). IR (KBr): ν 3321 cm^{-1} (w) ν(NH); 3083 (w) ν(CH); 2951 (vw) ν(CH); 1560 (s) ν(C=N); 832 and 828 (vs) $\nu(PF_6)$ and 557 (vs) δ(P–F). ^{1}H NMR (CD_3COCD_3): $\delta = 4.34$ (s, 5H, CpFe), 4.57 (br t, 2H, H_β–C_5H_4), 4.66 (br t, 2H, H_α–C_5H_4), 5.24 (s, 5H, $CpFe^+$), 6.73 (d, 2H, C_6H_4, $J_{H\text{-}H} = 6.9$ Hz), 6.46 (d, 2H, C_6H_4, $J_{H\text{-}H} = 6.9$ Hz), 8.10 (s, 1H, CH), 9.65 (br s, 1H, NH).

$[CpFe(\eta^6\text{–}C_6H_5)\text{–}NHN{=}CMe\text{–}(\eta^5\text{-}C_5H_4)FeCp]^+PF_6^-$, $[\mathbf{9}]^+PF_6^-$. To 63.7 mg (0.28 mmol) of acetylferrocene, $CpFe(\eta^5\text{-}C_5H_4\text{-CO-Me})$, dissolved in 5.0 ml of EtOH, 104.2 mg (0.28 mmol) of $[\mathbf{1}]^+PF_6^-$ and 3 drops of glacial acetic acid were added. The solution was refluxed for 7 h and the clean reaction mixture was then allowed to stand at room temperature. The red-orange solid formed was filtered off and washed with cold EtOH. Finally, the complex was recrystallized from CH_2Cl_2–Et_2O (1 : 1). Yield 124 mg (76%),

m.p. 168–9 °C (dec). $C_{23}H_{23}F_6Fe_2N_2P$ (584.11): calcd. C, 47.30; H, 3.97; found C, 47.02; H, 4.12. UV/Vis (CH_2Cl_2): λ_{max} ($\log\varepsilon$) 242 nm (4.30), 267 (4.11 sh), 291 (4.10 sh), 313 (4.16), 431 (3.35); (DMSO): λ_{max} ($\log\varepsilon$) 317 nm (4.12), 426 (3.29). IR (KBr): ν 3368, 3322 cm^{-1} (w) ν(NH); 3098 (w) ν(CH); 2996 (vw) ν(CH) 1554 (s) ν(C=N); 846, 832 (br, vs) $\nu(PF_6)$ and 558 (s) δ(P–F). ^1H NMR (CD_3COCD_3): $\delta = 2.33$ (s, 3H, CH_3), 4.37 (s, 5H, CpFe), 4.57 (br t, 2H, H_β–C_5H_4), 4.99 (br t, 2H, H_α–C_5H_4), 5.14 (s, 5H, $CpFe^+$), 6.22–6.57 (m, 5H, Ph), 8.95 (br s, 1H, NH). ^{13}C DEPT 135 NMR (75.45 MHz, CD_2Cl_2, 297 K): $\delta = 14.5$ (CH_3), 67.5 (C_β–C_5H_4), 69.8 (CpFe), 70.5 (C_α–C_5H_4), 70.7 (*o*-C C_6H_5), 76.2 ($CpFe^+$), 81.4 (*p*-C C_6H_5), 85.8 (*m*-C C_6H_5). The *trans* conformation is attributed on the basis of NOE difference spectra resulting in 12% enhancement of the N–H proton at δ 8.95 and of the H_α protons of the C_5H_4 ring at δ 4.99 after irradiation of the Me resonance at δ 2.33.

[CpFe(η^6-*p*-MeC$_6$H$_4$)–NHN=CMe–(η^5-C$_5$H$_4$)FeCp]$^+$PF$_6^-$, [10]$^+$PF$_6^-$. This orange complex was synthesized according to the procedure described above for [**9**]$^+$PF$_6^-$, using in this case 119 mg (0.52 mmol) of acetylferrocene and 41.0 mg (0.52 mmol) of [**2**]$^+$PF$_6^-$. Yield 204 mg (66%), m.p. 172–3 °C (dec). $C_{24}H_{25}F_6Fe_2N_2P$ (598.13): calcd. C, 48.19; H, 4.21; found C, 47.83; H, 4.41. UV/Vis (CH_2Cl_2): λ_{max} ($\log\varepsilon$) 242 nm (4.34), 267 (4.13 sh), 295 (4.15 sh), 309 (4.18), 431 (3.36); (DMSO): λ_{max} ($\log\varepsilon$) 314 nm (4.18), 426 (3.35). IR (KBr): ν 3348 cm^{-1} (w) ν(NH); 3096 (vw) ν(CH); 2921 (vw) ν(CH); 1564 (s) ν(C=N); 850 and 832(vs) $\nu(PF_6)$ and 558 (s) δ(P–F). ^1H NMR (CD_3COCD_3): $\delta = 2.17$ (s, 3H, CH_3), 2.41 (s, 3H, *p*-CH_3), 4.25 (s, 5H, CpFe), 4.45 (br t, 2H, H_β–C_5H_4), 4.88 (br t, 2H, H_α–C_5H_4), 4.96 (s, 5H, $CpFe^+$), 6.31 (d, 2H, C_6H_4, $J_{H\text{-}H} = 6.9$ Hz), 6.16 (d, 2H, C_6H_4, $J_{H\text{-}H} = 6.9$ Hz), 8.71 (br s, 1H, NH).

[CpFe(η^6-*p*-MeOC$_6$H$_4$)–NHN=CMe–(η^5-C$_5$H$_4$)FeCp]$^+$PF$_6^-$, [11]$^+$PF$_6^-$. This yellow complex was synthesized according to the procedure described above for [**9**]$^+$PF$_6^-$, using in this case 115 mg (0.50 mmol) of acetylferrocene and 201 mg (0.50 mmol) of [**3**]$^+$PF$_6^-$. Yield 192 mg (63%), m.p. 165–166 °C (dec). $C_{24}H_{25}F_6Fe_2N_2OP$ (614.13): calcd. C, 46.43; H, 4.10; found C, 46.84; H, 3.90. UV/Vis (CH_2Cl_2): λ_{max} ($\log\varepsilon$) 240 nm (4.40), 301 (4.25), 358 (3.82 sh), 425 (3.43 sh); (DMSO): λ_{max} ($\log\varepsilon$) 307 nm (4.17), 355 (3.81 sh), 414 (3.40). IR (KBr): ν 3332 cm^{-1} (w) ν(NH); 3102 (vw) ν(CH); 2932 (vw) ν(CH); 1560 (w) ν(C=N); 1252 (m) ν(C–O); 842 (vs) $\nu(PF_6)$, 558 (m) δ(P–F). ^1H NMR (CD_3COCD_3): $\delta = 2.21$ (s, 3H, CH_3), 3.96 (s, 3H, OCH_3), 4.18 (s, 5H, CpFe), 4.38 (br t, 2H, H_β–C_5H_4), 4.78 (br t, 2H, H_α–C_5H_4), 5.01 (s, 5H, $CpFe^+$), 6.28 (d, 2H, C_6H_4, $J_{H\text{-}H} = 7.2$ Hz), 6.18 (d, 2H, C_6H_4, $J_{H\text{-}H} = 7.2$ Hz), 8.69 (br s, 1H, NH).

X-ray structure determination for [9]$^+$PF$_6^-$

Suitable single crystals for X-ray diffraction studies were grown by slow diffusion of diethyl ether into a concentrated CH_2Cl_2 solution of [**9**]$^+$PF$_6^-$, at room temperature. An orange prism of this complex having dimensions of $0.33 \times 0.12 \times 0.10$ mm^3 was mounted on a glass fiber in a random orientation. Data collection was performed at room temperature on a Siemens Smart CCD diffractometer using graphite monochromated Mo-Kα radiation ($\lambda = 0.71073$) with a nominal crystal-to-detector distance of 4.0 cm. A hemisphere of data was collected on the basis of three ω-scan runs (starting $\omega = -28°$) at values $\varphi = 0$, 90, 180°, with the detector at $2\theta = 28°$. In each of these runs, frames (606, 435, 230, respectively) were collected at 0.3° intervals and for 40 s per frame. The diffraction frames were integrated using the SAINT package and corrected for absorption with SADABS.[34,35] The positions of the heavy atoms were determined by direct methods and successive difference electron density maps using the SHELXTL 5.10 software package[36] were done to locate the remaining atoms. Refinement was performed by the full-matrix least-squares method based on F^2. All non-hydrogen atoms were refined anisotropically. The positions of the aromatic hydrogens were generated geometrically, assigned isotropic thermal parameters and allowed to ride on their respective parent C atoms.

Crystallographic data for [**9**]$^+$PF$_6^-$: $C_{23}H_{23}F_6Fe_2N_2P$, $M_r = 584.10$, $a = 14.819(2)$, $b = 16.500(4)$, $c = 19.295(3)$ Å, $\beta = 95.679(12)°$, $u = 4694.7(14)$ Å^3, monoclinic, space group $P2_1/c$, $Z = 8$, 298(2) K, 7385 reflections collected, 4049 independent reflections [R(int) = 0.0491]. Convergence at conventional $R_1 = 0.0917$, $wR_2 = 0.1211$ (all data), 613 parameters.

CCDC reference number 167305. See http://www.rsc.org/suppdata/nj/b1/b107631k/ for crystallographic data in CIF or other electronic format.

Computational details

DFT calculations[37] were carried out using the Amsterdam Density Functional (ADF) program.[38] The Vosko–Wilk–Nusair parametrization[39] was used to treat electron correlation within the local density approximation (LDA). Calculations were also carried out at the nonlocal level, using the corrections to the exchange and correlation energies of Becke[40] and of Perdew[41] (BP), respectively. The numerical integration procedure applied for the calculations was developed by te Velde and Baerends.[37d] A triple-ζ Slater-type orbital (STO) basis set was used for Fe 3d and 4s. A single-ζ STO was used for Fe 4p. A double-ζ STO basis set was employed for H 1s, C and N 2s and 2p, extended with a single-ζ polarization function 2p for H and 3d for C and N. The frozen-core approximation was used to treat the core electrons.[37a] Full geometry optimizations were carried out on each complex, using the analytical gradient method implemented by Verluis and Ziegler.[42] Due to the large size of the computed compounds, only spin-restricted calculations were carried out for the open-shell species.

Acknowledgements

The authors gratefully acknowledge Prof. R. Llusar (Univ. Jaume I) for her helpful assistance with the X-ray analysis, and Prof. M. Tilset (University of Oslo) for stimulating discussions and comments. We greatly appreciate financial support for this work from the Fondo Nacional de Desarrollo Científico y Tecnológico, FONDECYT, Grant N° 1000281 (C. M.), the Programme International de Coopération Scientifique, CNRS-CONICYT [PICS N° 922 (2000-02)] (C. M., D. C., P. H., J.-R. H., S. K., J.-Y. S.), the Universidad Católica de Valparaíso and the Université de Rennes 1.

References

1 See, for example: (*a*) M. L. H. Green, S. R. Marder, M. E. Thompson, J. A. Bandy, D. Bloor, P. V. Kolinsky and R. J. Jones, *Nature* (*London*), 1987, **26**, 360; (*b*) D. R. Kanis, M. A. Ratner and T. J. Marks, *J. Am. Chem. Soc.*, 1990, **112**, 8203; (*c*) U. Behrens, H. Bussaard, U. Hagenau, J. Heck, E. Hendrickx, J. Körnich, J. G. M. van den Linden, A. Persoons, A. L. Spek, N. Veldman, B. Voss and H. Wong, *Chem. Eur. J.*, 1996, **2**, 98; (*d*) E. Hendrickx, A. Persoons, S. Samson and G. R. Stephenson, *J. Organomet. Chem.*, 1997, **542**, 295; (*e*) F. Coat, M. A. Guillevic, L. Toupet, F. Paul and C. Lapinte, *Organometallics*, 1997, **16**, 5988; (*f*) I. S. Lee, S. S. Lee, Y. K. Chung, D. Kim and N. W. Song, *Inorg. Chim. Acta*, 1998, **279**, 243; (*g*) W. Wenseleers, A. W. Gerbrandij, E. Goovaerts, M. H. Garcia, M. P. Robalo, P. J. Mendes, J. C. Rodrigues and A. Dias, *J. Mater. Chem.*, 1998,

8, 925; (*h*) G. G. A. Balavoine, J. C. Daran, G. Iftime, P. G. Lacroix, E. Manoury, J. A. Delaire, I. Maltey-Fanton and K. Nakatami, *Organometallics*, 1999, **18**, 21; (*i*) S. I. Lee, H. Seo and Y. K. Chung, *Organometallics*, 1999, **18**, 1091; (*j*) A. M. McDonagh, M. G. Humphrey, M. Samoc, B. Luther-Davies, S. Houbrechts, T. Wada, H. Sasabe and A. Persoons, *J. Am. Chem. Soc*., 1999, **121**, 1405; (*k*) E. Licandro, S. Maiorana, A. Papagni, P. Hellier, L. Capella, A. Persoons and S. Houbrechts, *J. Organomet. Chem*., 1999, **583**, 111; (*l*) T. Renouard, H. Le Bozec, S. Brasselet, I. Ledoux and J. Zyss, *Chem. Commun*., 1999, 871; (*m*) S. Le Stang, D. Lenz, F. Paul and C. Lapinte, *J. Organomet. Chem*., 1999, **572**, 189; (*n*) J. A. Mata, E. Falomir, R. Llusar and E. Peris, *J. Organomet. Chem*., 2000, **616**, 80; (*o*) J. A. Mata, S. Uriel, R. Llusar and E. Peris, *Organometallics*, 2000, **19**, 3797; (*p*) J. P. Tranchier, R. Chavignon, D. Prim, A. Auffrant, Z. F. Plyta, F. Rose-Munch and E. Rose, *Tetrahedron Lett*., 2000, **41**, 3607; (*q*) J. A. Mata, E. Peris, I. Asselberghs, R. Van-Boxel and A. Persoons, *New J. Chem*., 2001, **25**, 299; (*r*) R. D. A. Hudson, A. R. Manning, D. F. Nolan, I. Asselberghs, R. Van-Boxel, A. Persoons and J. F. Gallagher, *J. Organomet. Chem*., 2001, **619**, 141; (*s*) F. Le Guen, P. Le Poul, B. Caro, R. Pichon and N. Kervarec, *J. Organomet. Chem*., 2001, **626**, 37.

2 (*a*) E. Goovaerts, W. E. Wenseleers, M. H. Garcia and G. H. Cross, in *Handbook of Advanced Electronic and Photonic Materials and Devices*, ed. H. S. Nalwa, Academic Press, New York, 2001, vol. 9, p. 127; (*b*) J. J. Wolff and R. Wortmann, in *Advances in Physical Organic Chemistry*, ed. D. Bethell, Academic Press, New York, 1999, vol. 32, p. 121; (*c*) J. Heck, S. Dabek, T. Meyer-Friedrichsen and H. Wong, *Coord. Chem. Rev*., 1999, **190–192**, 1217; (*d*) I. R. Whittall, M. McDonagh and M. G. Humphrey, *Adv. Organomet. Chem*., 1998, **42**, 291; (*e*) N. J. Long, *Angew. Chem., Int. Ed. Engl*., 1995, **34**, 21.

3 (*a*) J. A. Mata, S. Uriel, E. Peris, R. Llusar, S. Houbrechts and A. Persoons, *J. Organomet. Chem*., 1998, **562**, 197; (*b*) Z. F. Plyta, D. Prim, J. P. Tranchier, F. Rose-Munch and E. Rose, *Tetrahedron Lett*., 1999, **40**, 6769; (*c*) T. J. J. Müller, *Tetrahedron Lett*., 1997, **38**, 1025; (*d*) T. J. J. Müller, *J. Organomet. Chem*., 1999, **578**, 95; (*e*) J. P. Tranchier, R. Chavignon, D. Prim, A. Auffrant, J. G. Planas, F. Rose-Munch, E. Rose and G. R. Stephenson, *Tetrahedron Lett*., 2001, **42**, 3311; (*f*) D. Prim, A. Auffrant, Z. F. Plyta, J. P. Tranchier, F. Rose-Munch and E. Rose, *J. Organomet. Chem*., 2001, **624**, 124.

4 T. Farrell, T. Meyer-Friedrichsen, M. Malessa, D. Haase, W. Saak, I. Asselberghs, K. Wostyn, K. Clays, A. Persoons, J. Heck and A. R. Manning, *J. Chem. Soc., Dalton Trans*., 2001, 29.

5 (*a*) H. A. Trujillo, C. M. Casado, J. Ruiz and D. Astruc, *J. Am. Chem. Soc*., 1999, **121**, 5674; (*b*) C. Lambert, W. Gaschler, M. Zabel, R. Matschiner and R. Wortmann, *J. Organomet. Chem*., 1999, **592**, 109.

6 D. Astruc, *Acc. Chem. Res*., 1997, **30**, 383.

7 C. Manzur, E. Baeza, L. Millán, M. Fuentealba, P. Hamon, J.-R. Hamon, D. Boys and D. Carrillo, *J. Organomet. Chem*., 2000, **608**, 126.

8 (*a*) D. Astruc, *Tetrahedron*, 1983, **39**, 4027; (*b*) D. Astruc, *Top. Curr. Chem*., 1991, **160**, 47; (*c*) A. S. Abd-El-Aziz and S. Bernardin, *Coord. Chem. Rev*., 2000, **203**, 219; (*d*) P. C. B. Gomes, E. J. S. Vichi, P. J. S. Moran, A. Federman Neto, M. L. Maroso and J. Miller, *Organometallics*, 1996, **15**, 3198.

9 C. Manzur, L. Millán, M. Fuentealba, J.-R. Hamon and D. Carrillo, *Tetrahedron Lett*., 2000, **41**, 3615.

10 (*a*) C. López, R. Bosque, X. Solans and M. Font-Bardia, *J. Organomet. Chem*., 1997, **547**, 309; (*b*) C. López and J. Granell, *J. Organomet. Chem*., 1998, **555**, 211.

11 H. Günther, in *La Spectroscopie de RMN: Principes de Base, Concepts et Applications de la Spectroscopie de Résonance Magnétique Nucléaire du Proton et du Carbone 13 en Chimie*, Masson, Paris, 1994, pp. 330–334.

12 *Comprehensive Organometallic Chemistry II*, ed. E. W. Abel, F. G. A. Stone and G. Wilkinson, Pergamon Press, Oxford, 1995, vol. 9.

13 For structurally characterized $[CpFe(arene)]^+$ mixed sandwiches see, for example: (*a*) J.-R. Hamon, J.-Y. Saillard, A. Le Beuze, M. J. McGlinchey and D. Astruc, *J. Am. Chem. Soc*., 1982, **104**, 7549; (*b*) See also refs 7, 15 and 19*b*.

14 For structurally characterized ferrocene-based π-bridged systems, see, for example: refs 3*a* and 4.

15 (*a*) J.-L. Fillaut, R. Boese and D. Astruc, *Synlett*, 1992, 55; (*b*) S. Subramanian, L. Wang and M. J. Zaworotko, *Organometallics*, 1993, **12**, 310; (*c*) Y. Ishii, M. Kawaguchi, Y. Ishino, T. Aoki and M. Hidai, *Organometallics*, 1994, **13**, 5062.

16 I. Chavez, A. Alvarez-Carena, E. Molins, A. Roig, W. Maniukiewicz, A. Arancibia, V. Arancibia, H. Brand and J. M. Manríquez, *J. Organomet. Chem*., 2000, **601**, 126.

17 (*a*) M.-H. Delville, F. Robert, P. Gouzerh, J. Linares, K. Boukheddaden, F. Varret and D. Astruc, *J. Organomet. Chem*., 1993, **451**, C10; (*b*) S. Rittinger, D. Buchholz, M.-H. Delville-Desbois, J. Linarès, F. Varret, R. Boese, L. Zolnai, G. Huttner and D. Astruc, *Organometallics*, 1992, **11**, 1454.

18 (*a*) M. Lacoste, F. Varret, L. Toupet and D. Astruc, *J. Am. Chem. Soc*., 1987, **109**, 6504; (*b*) D. Astruc, M. Lacoste and L. Toupet, *J. Chem. Soc., Chem. Commun*., 1990, 558.

19 A similar structural behavior is noted for related crystallographically characterized π-coordinated arenes bearing a benzylic nitrogen atom: (*a*) see ref. 7; (*b*) V. M. Lynch, S. N. Thomas, S. H. Simonses, A. Piórko and R. G. Sutherland, *Acta Crystallogr., Sect. C*, 1986, **42**, 1144; (*c*) J.-Y. Saillard, D. Grandjean, P. Le Maux and G. Jaouen, *Nouv. J. Chim*., 1981, **5**, 153; (*d*) see also ref. 15*c*.

20 For theoretical work see: J. Ruiz, F. Ogliaro, J.-Y. Saillard, J.-F. Halet, F. Varret and D. Astruc, *J. Am. Chem. Soc*., 1998, **120**, 11 693.

21 The C–N bond distances are roughly halfway between those of a single and a double bond. A. G. Orpen, L. Brammer, F. H. Allen, D. Kennard, D. G. Watson and R. Taylor, *J. Chem. Soc., Dalton Trans*., 1989, S1.

22 C. Manzur, M. Fuentealba, D. Carrillo, D. Boys and J.-R. Hamon, *Bol. Soc. Chil. Quim*., 2001, **46**, 409.

23 D. Astruc, *Chem. Rev*., 1988, **88**, 1189.

24 Preliminary cyclic voltammetry experiments on mononuclear hydrazone derivatives seem to confirm this influence of the hydrazone backbone effect on the peak potential shifts. Under standard conditions (CH_3CN, 20 °C, 0.1 M n-$Bu_4N^+PF_6^-$, $v = 0.1$ V s^{-1}), complex $[CpFe(\eta^6\text{-}C_6H_5\text{–}NHNCMe_2)]^+PF_6^-$ exhibits an irreversible reduction wave at −1.42 V *vs.* Ag/AgCl, whereas the neutral ferrocenyl hydrazone $CpFe[\eta^5\text{-}C_5H_4\text{–}C(Me)NNHPh]$ shows a quasi-reversible oxidation wave at $E^0 = 0.47$ V *vs.* Ag/AgCl ($\Delta E_p = 150$ mV), corroborating the DFT results. C. Manzur, M. Fuentealba, J.-R. Hamon and D. Carrillo, unpublished work.

25 P. Zanello, in *Ferrocenes*, ed. A. Togni and T. Hayashi, VCH, New York, 1995, pp. 317–424.

26 (*a*) H. Wong, T. Meyer-Friedrichsen, T. Farrell, C. Mecker and J. Heck, *Eur. J. Inorg. Chem*., 2000, 631; (*b*) see also ref. 4 and references cited therein; (*c*) T. J. J. Müller, A. Netz and M. Ansorge, *Organometallics*, 1999, **18**, 5066; (*d*) J. A. Campo, M. Cano, J. V. Heras, C. Lopez-Garabito, E. Pinilla, R. Torres, G. Rojo and F. Agullo-Lopez, *J. Mater. Chem*., 1999, **9**, 899.

27 S. Barlow, H. E. Bunting, C. Ringham, J. C. Green, G. U. Bublitz, S. G. Boxer, J. W. Perry and S. R. Marder, *J. Am. Chem. Soc*., 1999, **121**, 3715.

28 D. R. Kanis, M. A. Ratner and T. J. Marks, *J. Am. Chem. Soc*., 1992, **114**, 10 338.

29 (*a*) W. H. Morrison, E. Y. Ho and D. N. Hendrickson, *Inorg. Chem*., 1975, **14**, 500; (*b*) J.-R. Hamon, D. Astruc and P. Michaud, *J. Am. Chem. Soc*., 1981, **103**, 758.

30 (*a*) Y. S. Sohn, D. N. Hendrickson and H. B. Gray, *J. Am. Chem. Soc*., 1971, **93**, 3603; (*b*) Y. Yamaguchi and C. Kutal, *Inorg. Chem*., 1999, **38**, 4861.

31 (*a*) D. L. Braden and D. T. Tyler, *Organometallics*, 2000, **19**, 1175; (*b*) F. Ogliaro, J.-F. Halet, D. Astruc and J.-Y. Saillard, *New J. Chem*., 2000, **24**, 257.

32 A. L. Van Geet, *Anal. Chem*., 1970, **42**, 679.

33 I. U. Khand, P. L. Pauson and E. E. Watts, *J. Chem. Soc. C*, 1969, 2261.

34 *SAINT* (ver. 5.0), Bruker Analytical X-ray Systems, Inc., Madison, WI, 1998.

35 G. M. Sheldrick, SADABS, Empirical Absorption Program, University of Göttingen, Göttingen, Germany.

36 *SHELXTL Reference Manual* (ver. 5.1), Bruker Analytical X-ray Systems, Inc., Madison, WI, 1997 .

37 (*a*) E. J. Baerends, D. E. Ellis and P. Ros, *Chem. Phys*., 1973, **2**, 41; (*b*) E. J. Baerends and P. Ros, *Int. J. Quantum Chem*., 1978, **S12**, 169; (*c*) P. M. Boerrigter, G. te Velde and E. J. Baerends, *Int. J. Quantum Chem*., 1988, **33**, 87; (*d*) G. te Velde and E. J. Baerends, *J. Comput. Phys*., 1992, **99**, 84.

38 Amsterdam Density Functional (ADF) program, ver. 2.3, Vrije Universiteit, Amsterdam, The Netherlands, 1996.

39 S. D. Vosko, L. Wilk and M. Nusair, *Can. J. Chem*., 1990, **58**, 1200.

40 (*a*) A. D. Becke, *J. Chem. Phys*., 1986, **84**, 4524; (*b*) A. D. Becke, *Phys. Rev. A*, 1988, **38**, 3098.

41 (*a*) J. P. Perdew, *Phys. Rev. B*, 1986, **33**, 8882; (*b*) J. P. Perdew, *Phys. Rev. B*, 1986, **34**, 7406.

42 L. Verluis and T. Ziegler, *J. Chem. Phys*., 1988, **88**, 322.